Variational Assimilation of GPS Precipitable Water Vapor and Hourly Rainfall Observations for a Meso-β Scale Heavy Precipitation Event During the 2002 Mei-Yu Season

ZHANG Meng[*1,3] (张 盟), NI Yunqi[2] (倪允琪), and ZHANG Fuqing[3] (张福青)

[1]*Department of Atmospheric Sciences, Nanjing University, Nanjing* 210093

[2]*State Key Laboratory of Severe Weather, Chinese Academy of Meteorological Sciences, Beijing* 100081

[3]*Department of Atmospheric Sciences, Texas A & M University, College Station, Texas* 77843-3150*, USA*

ABSTRACT

Recent advances in Global Positioning System (GPS) remote sensing technology allow for a direct estimation of the precipitable water vapor (PWV) from delayed signals transmitted by GPS satellites, which can be assimilated into numerical models with four-dimensional variational (4DVAR) data assimilation. A mesoscale model and its 4DVAR system are used to access the impacts of assimilating GPS-PWV and hourly rainfall observations on the short-range prediction of a heavy rainfall event on 20 June 2002. The heavy precipitation was induced by a sequence of meso-β-scale convective systems (MCS) along the mei-yu front in China.

The experiments with GPS-PWV assimilation successfully simulated the evolution of the observed MCS cluster and also eliminated the erroneous rainfall systems found in the experiment without 4DVAR assimilation. Experiments with hourly rainfall assimilation performed similarly both on the prediction of MCS initiation and the elimination of erroneous systems, however the MCS dissipated much sooner than it did in observations. It is found that the assimilation-induced moisture perturbation and mesoscale low-level jet are helpful for the MCS generation and development. It is also discovered that spurious gravity waves may post serious limitations for the current 4DVAR algorithm, which would degrade the assimilation efficiency, especially for rainfall data. Sensitivity experiments with different observations, assimilation windows and observation weightings suggest that assimilating GPS-PWV can be quite effective, even with the assimilation window as short as 1 h. On the other hand, assimilating rainfall observations requires extreme cautions on the selection of observation weightings and the control of spurious gravity waves.

Key words: GPS, precipitable water vapor, four-dimensional variational assimilation, meso-β-scale convective system

1. Introduction

Atmospheric water vapor plays a significant role in numerical weather predictions (NWP) of heavy rainfall systems, because its distribution is directly related to the formation of clouds and precipitation and also involved in determining the various thermodynamic and microphysical processes for the initiation and development of strong convections. Therefore, the improved characterization of the moisture field would result in remarkable improvements on quantitative precipitation forecast (QPF) skills. On the other hand, even though most severe weathers that result in heavy rainfall are caused by meso-β-scale convective systems (MCS) with the scales from 20 km to 200 km and not longer than 24-h lifetimes, in fact, there is a lack of measurements of their moisture distribution in conventional observations, such as radiosondes, whose spatial and temporal resolutions are respectively limited at about 200 km and 12 hours. Consequently, it is difficult for us to determine detailed mesoscale structures of these convective systems for numerical models to

*E-mail: mzhang@tamu.edu

establish reasonable initial conditions (IC) and then accurately forecast these heavy rainfall events.

Coinciding with the recent developments in the use of Global Positioning System (GPS) in atmospheric remote sensing, a new technology, dependent on the ground-based GPS receivers, provides us a type of high-resolution (both on spatial and temporal scales), high-accuracy and low-cost measurements for moisture field. Based on the delayed GPS signals, we can retrieve the total amount of the vertically integrated atmospheric water vapor on the zenithal path of the receiver, which is usually defined as precipitable water vapor (PWV) (Bevis et al., 1992; Duan et al., 1996). Since PWV is the source of rainfall, it is very desirable to assimilate this new type of observations into mesoscale models to improve MCS QPF, where four-dimensional variational (4DVAR) data assimilation is one of the most promising methods.

4DVAR was first applied to simplified dynamical models (Le Dimet and Talagrand, 1986; Courtier and Talagrand, 1987) and subsequently developed for more sophisticated models (Thepaut et al., 1993; Navon et al., 1992; Zou et al., 1993, 1995; Zupanski, 1993), while the continually increasing computational resources began to allow its implementation in high-resolution mesoscale models. Since 1992, many encouraging attempts have been made at assimilating GPS-PWV data for heavy rainfall predictions. Kuo et al. (1993) used a newtonian relaxation (nudging) method to ingest the PWV data into a mesoscale model. The 4DVAR technique was later used by Kuo et al. (1996) to directly assimilate GPS-PWV data into the fifth-generation Pennsylvania State University-National Center for Atmospheric Research (PSU-NCAR) Mesoscale Model (MM5). In the meantime, other studies examined the effectiveness of 4DVAR assimilation on rainfall observations (Zupanski and Mesinger, 1995; Zou and Kuo, 1996). Guo et al. (2000) used the MM5 4DVAR system to investigate the correlations between GPS-PWV assimilation and model-predicted rainfall patterns, which concluded that the ground-based GPS data assimilation had a significant impact on the short-range rainfall prediction for a squall line. More recently, De Pondeca et al. (2001) and Ha et al. (2003) began to directly assimilate zenithal or slant-path delayed GPS signals with the MM5 4DVAR system for various severe convective systems.

Despite the advancements in the 4DVAR technique on GPS-PWV and rainfall data assimilations, there have been few studies focusing on the meso-β-scale convective systems that usually develop along the mei-yu front in China. The mei-yu front (Baiu in Japan) is a qausi-stationary frontal system extending from eastern China to southern Japan, which is one of the most significant synoptic circulations in the East Asian monsoon region during the rainy season (usually called mei-yu season) (Ding, 1992). According to many observational and simulated evidences, people find that most severe heavy rainfalls, even flash floods in the mei-yu season, are often associated with well-organized MCS clusters, which are embedded within and propagate along the mei-yu front (Chen et al., 1998; Davison et al., 1998; Zhang et al., 2003; Moteki et al., 2004; Sun et al., 2005). However, the QPF skill is partially limited by the shortage of the observations on these mesoscale systems in China, where the sophisticated data assimilations are also needed (Zhang and Ni, 2005). Fortunately, a ground-based GPS observational network (14 sites) was built over the lower reaches of the Yangtze River in June 2002, allowing for continued PWV observations with 30-min intervals. The field experiment of China Heavy Rain Experiment and Study (CHeRES) program provides us additional GPS-PWV measurements (6 sites) and hourly rainfall observations (137 sites) during its intensive observation period (IOP) in 2002, which provides a good opportunity to examine the impacts of GPS-PWV and rainfall data assimilations on the MCS heavy rainfall predictions.

In this study, we mainly focus on one such MCS cluster located within the observational network between 1200 UTC and 2400 UTC 20 June 2002 and conduct a series of 4DVAR experiments with alternative selections of observations, different assimilation windows and error weightings: (1) to compare the different effects between GPS-PWV and rainfall assimilations in the IC adjustments and their subsequent MCS forecasts; (2) to examine the existence and possible reasons of spurious gravity waves problem in the current 4DVAR algorithm; and (3) to examine the sensitivity of 4DVAR for moisture predictions. In section 2, we give out a synoptic overview of the case chosen in this study. Section 3 introduces the observational network, 4DVAR cost functions, forecast models and numerical experiments in our study. The forecast verifications are shown in section 4. Section 5 presents the initial condition adjustments both physically and numerically. In section 6, we analyze the forecast sensitivities to the GPS-PWV and rainfall assimilations. Conclusions and discussions are given in section 7.

2. Brief description of synoptic case

A cluster of strong, heavy-precipitating, meso-β-scale convective systems on the mei-yu front that occurred in the lower reaches of Yangtze River during 1200 UTC–2400 UTC 20 June 2002 was chosen for
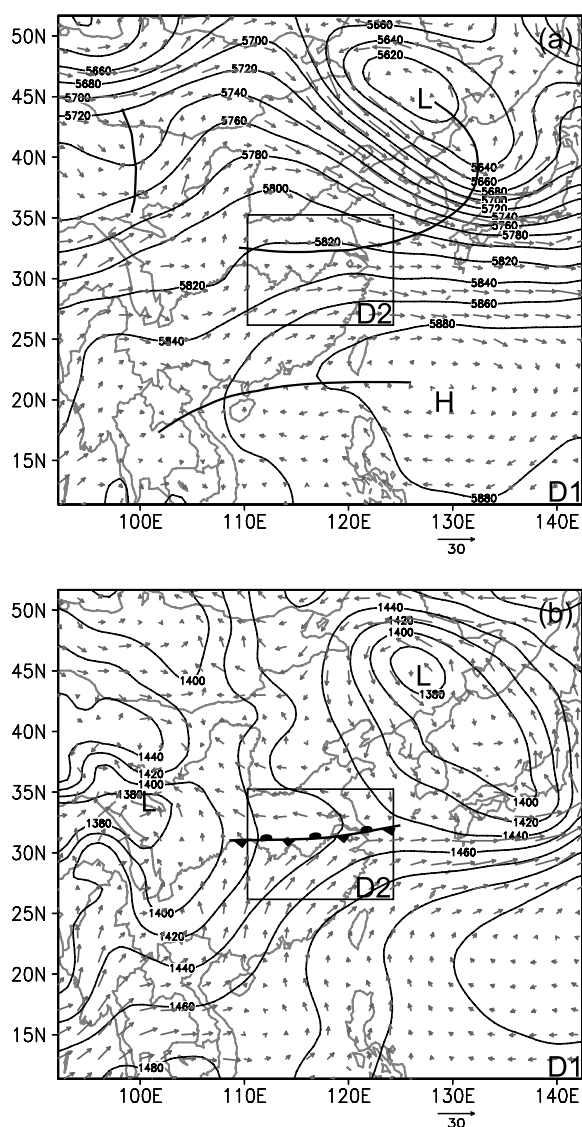
Fig. 1. The analysis of the geopotential height and wind fields at 1200 UTC 20 June 2002, (a) for 500 hPa and (b) for 850 hPa. The values are interpolated from the NCEP FNL $1° \times 1°$ data and shown on the coarse (54-km) grid domain with the fine (18-km) nested domain in the box. The contour interval for the geopotential height is 20 m and the isotach is 30 m s^{-1}. The shear and ridge lines are draw at (a), and the surface mei-yu front is marked at (b).

this study. At 500 hPa, 1200 UTC 20 June 2002 (Fig. 1a), the ridge line of strong western Pacific subtropical high pressure (WPSH) nearly paralleled to the 20°N line, and the 5880-m line (height contour), which is usually used to define the area of WPSH, reached to 25°N and 117°E. On the northwest side of WPSH, there was an intensive southwestward flow between 25°N to 30°N. In the middle latitudes, a major trough was located at Sea of Japan and crossed over the Ko-

rean Peninsula. The southern part of this trough extended to form a weak shear line along the Yangtze River. There was another short-wave trough located at 100°E on the western part of the major system. In the lower levels, the shear line was more clearly shown at 850 hPa (Fig. 1b). A strong southwesterly synoptic-scale low-level jet (LLJ) at the southern side of the shear line, with wind speed over 15 m s^{-1}, extended to the South China Sea, which brought abundant warm moist air to the middle and lower reaches of the Yangtze River. Under the shear line, the surface mei-yu front developed and was located along the 32°N line. In the meantime, there was a synoptic-scale vortex named southwestern vortex (SWV) centered around (34°N, 100°E) on the southwestern part of China. The SWV is usually associated with heavy rainfall in the mei-yu season (Ding, 1992). In summary, the synoptic pattern is very typical of severe rainfall events during mei-yu season in China.

Figure 2 illustrates the evolution of the MCSs along the mei-yu front within a limited-area observational network over the lower reach of the Yangtze River which included two Doppler radars located at Hefei (58321) and Ma'anshan (58336), respectively, and 137 auto weather stations (AWS). In this case, we regard the strong convection as the area where column maximum reflectivity is over 40 dB(Z). Outside the radar scope, the localized rainfall centers are used to track the MCSs (Fig. 2).

At 1300 UTC 20 June 2002, the first MCS, labeled "A", generated at (31.5°N, 116°E) near the Dabie Mountains with little precipitation (Fig. 2a). This MCS quickly moved eastward and strengthened in the following few hours. At 1700 UTC, the MCS centered at (30.8°N, 117.5°E) with maximum hourly accumulated precipitation over 20 mm (Fig. 2b). Afterward, MCS A continued on an eastward path and started to weaken. During this period, two other strong MCSs respectively labeled "B" and "C" were produced on the southern side of MCS A over the Huangshan Mountain area. At 2100 UTC, the center of the weakening MCS A arrived at (31.8°N, 119.2°E) with maximum hourly precipitation of 10 mm. In the meantime, MCSs B and C, which were respectively located at (31°N, 118.5°E) and (30°N, 117.5°E), developed quickly and generated more precipitation than MCS A. Both MCSs A and B kept on drifting eastward and moved out of the scope of the radars at 2400 UTC without apparent reduction in their precipitation. MCS C became the most intensive system at this time, which produced over 20 mm hourly rainfall and centered at (31°N, 118.5°E) (Fig. 2d). By this time, the three MCSs (A, B, and C) had formed a clustered rainfall pattern along the 31.5°N line.
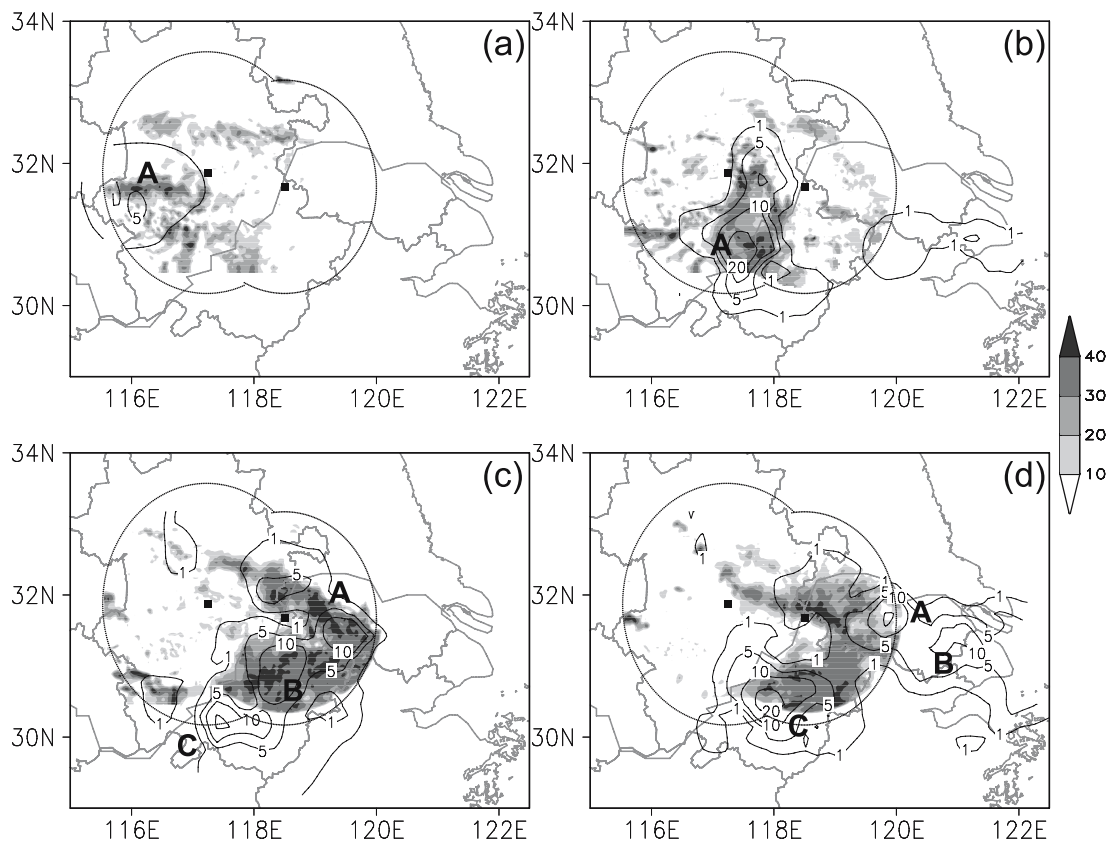
Fig. 2. Observed column maximum radar reflectivity images (shaded) and 1-hour accumulated precipitation ending at (a) 1300 UTC, (b) 1700 UTC, (c) 2100 UTC, (d) 2400 UTC 20 June 2002. The contour interval is 10 dB(Z) for radar reflectivity, and the contour levels for rainfall are 1, 5, 10, 20, 40 mm. The MCSs are marked as A, B, C for convenience.

3.   Observations and experiment design

3.1   *Observational network*

Most of the observations used in this study were provided by the field experiment of the CHeRES program during its IOP in 2002, which included 6 sites of GPS-PWV, 137 sites of hourly rainfall, 12 sites of enhanced radiosondes (available at 0000 UTC, 0600 UTC, 1200 UTC, and 1800 UTC) and 2 sites of Doppler radar observations. There were also another 14 sites of GPS-PWV associated with the Shanghai GPS Comprehensive Application Network (SGCAN). Figure 3 indicates the distribution of this mesoscale observational network in the experiment area.

A total of 20 ground-based GPS receivers in the lower reach of the Yangtze River were used, which covered an area of four provinces including Anhui, Jiangsu, Shanghai and Zhejiang. The signals transmitted from GPS satellites to these receivers are refracted and delayed by the atmosphere during their propagation. Accordingly, if we obtain the history of these delayed signals from a certain GPS receiver, the PWV

variation may be estimated using the retrieval method (Bevis et al., 1992; Duan et al., 1996). The GPS-PWV measurements are believed to have sufficient accuracy and stability under all weather conditions (Braun et al., 2001). To verify the credibility of PWV observations from the 20 ground-based GPS sites used in this study (Fig. 3), we calculated the root-mean square (RMS) difference between the GPS-PWV observations and those derived from radiosondes at the same sites, such as Shanghai (58362) and Hangzhou (58457). The RMS error was less than 4 mm during the four summer and autumn months of 2002, which is considered to be relatively low.

3.2   *MM5 4DVAR system*

The PSU-NCAR mesoscale model MM5 (Grell et al., 1994) and its 4DVAR system (Zou et al., 1997) were used in this study. The MM5 is a non-hydrostatic model with terrain-following vertical sigma coordinates. The 4DVAR system is based on an earlier version of MM5 (MM5v1) and has four major components, namely the nonlinear forecast model (NFM),
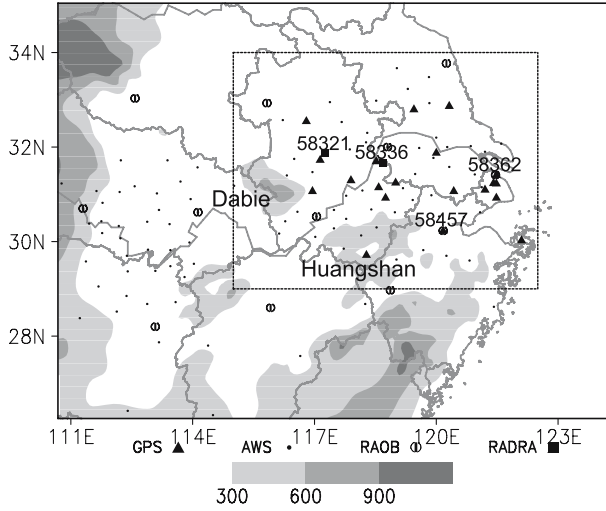
Fig. 3. The distribution of observations on the fine domain used in the experiments. The triangle is ground-based GPS receiver, the small dot is AWS for rainfall, the square is radar and the big dot is radiosonde. The contour interval for the terrain height (shaded) is 300 m, and the intensive observational area (Fig. 2) is limited by dashed line.

tangent linear model (TLM), adjoint model (ADM) and the minimization scheme. The tangent linear and adjoint models are directly coded from MM5v1. A limited-memory quasi-Newton method (L-BFGS) (Liu and Nocedal, 1989) was used in the minimization process for this 4DVAR system.

In 4DVAR, the major objective is to seek an optimal initial condition by minimizing the cost function (CF) within a certain time window by using multiple observations, error statistics, full model dynamics and physics. The cost function J can be expressed as (Zou et al., 1997):

$$
\begin{aligned}
J(\boldsymbol{X}_0) = J_{\mathrm{b}} + J_{\mathrm{obs}} = &\frac{1}{2}(\boldsymbol{X}_0 - \boldsymbol{X}_{\mathrm{b}})^{\mathrm{T}}\boldsymbol{B}^{-1}(\boldsymbol{X}_0 - \boldsymbol{X}_{\mathrm{b}}) + \\
&\frac{1}{2}\sum_{i=1}^{n}\{\boldsymbol{H}[\boldsymbol{X}(t_i)] - \boldsymbol{Y}_{\mathrm{obs}}(t_i)\}^{\mathrm{T}} \times \\
&O^{-1}\{\boldsymbol{H}[\boldsymbol{X}(t_{\mathrm{i}})] - \boldsymbol{Y}_{\mathrm{obs}}(t_i)\} \,,
\end{aligned}
\tag{1}
$$

where J can be divided into J_{b} and J_{obs}, which are weighted by the inverse of the background error covariance ($\boldsymbol{B}^{-1}$) and the observational error covariance (O^{-1}), respectively, $\boldsymbol{H}$ is the observational operator. In our study, $\boldsymbol{B}^{-1}$ is diagonal and obtained by taking the inverse of the squared maximum differences between the two forecasts in the assimilation window (Parrish and Derber, 1992). This is to say, the background error statistics of the current 4DVAR system does not account for the spatial correlations between

the different model variables and the flow-dependent variations of the covariance matrixes.

3.3 *Experiment design*

In this study, a total of nine experiments (Table 1) including a control experiment (CNTL) along with a series of 4DVAR experiments using different observations, assimilation windows and weightings were conducted. Due to the limited computational resources, all assimilation experiments were performed over a 58×76 grid mesh domain with a 18-km grid distance (Fig. 3), which was driven by hourly lateral boundary conditions (LBC) from a 86×86 54-km coarse domain output without 4DVAR (Fig. 1). Hence it is a one-way nested model configuration running on MM5 and its 4DVAR models. There were 15 vertical layers with a variable resolution that was higher near the ground.

We first ran a 12-h forecast on the coarse domain from 1200 UTC to 2400 UTC 20 June 2002, whose IC and LBC were interpolated from the $1° \times 1°$ NCEP Global Final Analysis (FNL) at 6-h intervals. The hourly forecast outputs of the coarse domain provided the LBCs for all experiments on the fine domain, including both the forecast and 4DVAR runs (Fig. 4). The CNTL experiment initialized at 1200 UTC 20 June 2002 is a standard 12-h simulation using the MM5 version 3 (MM5v3) without data assimilation. Since the CNTL also derived its IC from the NCEP FNL analysis, it reflects the typical accuracy of the forecast model initialized by the operational analysis and thus is used as a benchmark for experiments with 4DVAR assimilation.

Experiments "PW1", "PW3" and "PW6" assimilated GPS-PWV observations every 30-min, beginning at 1200 UTC 20 June 2002 with total assimilation windows of 1, 3 and 6 h, respectively (Fig. 4). The weighting of observations O^{-1} was defined by a diagonal matrix with constant element of 30 $(\mathrm{g\ cm}^{-2})^{-2}$ (refer to Kuo et al., 1996; Guo et al., 2000). Similarly, experiments "Rain1", "Rain3", and "Rain6" assimilated hourly rainfall observations beginning at 1200 UTC with total assimilation windows of 1, 3 and 6 h, respectively (Fig. 4). The weighting of observations O^{-1} was defined as 100.0 cm^{-2} which corresponded to an error of 0.1 cm on rainfall measurements. Experiment "Rain3L" is the same as "Rain3" except that observation weighting O^{-1} was modified to 11.1 cm^{-2} (Guo et al., 2000) so as to test the sensitivity of rainfall assimilation to assumed observational error weightings. Experiment "PWRain" assimilated both GPS-PWV and hourly rainfall observations with the total assimilation window of 3 h, similar to PW3 and Rain3.

For each experiment, a 12-h MM5v3 forecast was initialized with the 4DVAR-adjusted ICs at 1200 UTC

Table 1. List of data assimilation experiments.

EXPT	Obs Variable	Assimilation Window (hour)	Obs Weighting
CNTL	N/A	N/A	N/A
PW1	GPS/PWV	1	30 $(g\ cm^{-2})^{-2}$
PW3	GPS/PWV	3	30 $(g\ cm^{-2})^{-2}$
PW6	GPS/PWV	6	30 $(g\ cm^{-2})^{-2}$
Rain1	Hourly Rainfall	1	100 cm^{-2}
Rain3	Hourly Rainfall	3	100 cm^{-2}
Rain3L	Hourly Rainfall	3	11.1 cm^{-2}
Rain6	Hourly Rainfall	6	100 cm^{-2}
PWRain	GPS/PWV and Rainfall	3	30 $(g\ cm^{-2})^{-2}$ and 11.1 cm^{-2}
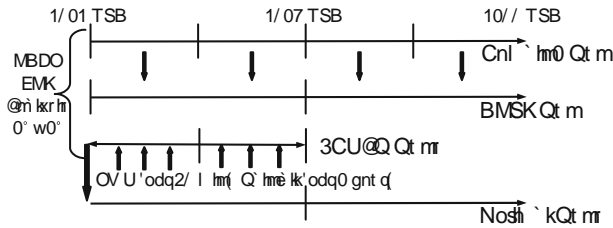
Fig. 4. Schematic diagram of the experimental design for control, optimal and assimilation runs.

in comparison to the CNTL simulation without 4DVAR assimilation. The Balckadar planetary boundary layer (PBL) parameterization (Blackadar, 1979; Zhang and Anthes, 1982), mixed-phase moisture scheme (Reisner et al., 1998) and cloud radiation scheme (Dudhia, 1989) were employed in both the coarse and fine domain forecasts. The Grell cumulus parameterization schemes (Grell, 1993) were used for the 18-km fine domain, while the Anthes-Kuo scheme (Kuo, 1974) was used for the 54-km coarse domain. The 4DVAR system employed the same model physics except for using the simple ice microphysics scheme (Dudhia, 1989). In the 4DVAR rainfall assimilation experiments, the Anthes-Kuo scheme was used to obtain better convergence in the minimization of the cost function J, as in Zou and Kuo (1996).

4. Results from the experiments

4.1 *Performance in the minimization process*

Figure 5 displays the variations of the cost function J and its associated gradient norm G in respect to the number of iterations in the 4DVAR minimization process for experiments PW3 and Rain3. The values of J and G in both experiments deceased rapidly for the first 5–10 iterations and then approached a low magnitude near saturation. The cost function J in PW3 decreased more rapidly than Rain3 and reached a magnitude of only 1% of the initial value after 30 iterations with G approaching zero. J could be further decreased

if the minimization process were allowed to continue. For Rain3, the value of J reduced to 10% of the initial value with G also reaching a very low level after 30 iterations but no further reduction in J was observed afterwards. In other 4DVAR experiments, the CFs and their corresponding gradient norms all converged to similar levels (i.e., 1% for J in PWV assimilations and 10% for rainfall assimilations). However, if the Grell cumulus scheme was used for hourly rainfall data assimilation, the CF only reduced to 95% of its initial value. The reasons for the non-convergence in 4DVAR are complex: it might be a function of model physics, resolutions, data types or observational error weightings (Guo et al., 2000) as well as the influence of the different weather events. Thus, the Anthes-Kuo scheme was used for the hourly rainfall assimilations because of its minimization efficiency.

4.2 *PWV error variation*

Since the GPS-derived PWV data represent the atmospheric moisture distribution over the experiment area, which is a major focus of our study, we evaluated the model performance in each experiment via comparison between ground-based GPS-PWV observations and the model-predicted values at the same observational sites in terms of the RMS error and the correlation coefficient (Fig. 6). The model-predicted PWV is calculated through:

$$PWV = \frac{p^*}{g} \sum_{k=1}^{K} q(k)\Delta\sigma(k) , \qquad (2)$$

where p^* is the difference between the surface and model top pressures (100 hPa), $q(k)$ is the specific humidity and $\Delta\sigma(k)$ is the mean thickness at the kth sigma layer, while K denotes the total number of sigma layers.

Except for Rain1, all 4DVAR experiments achieved a lower RMS error and a higher correlation coefficient than the CNTL experiment, especially in the first 6 h,
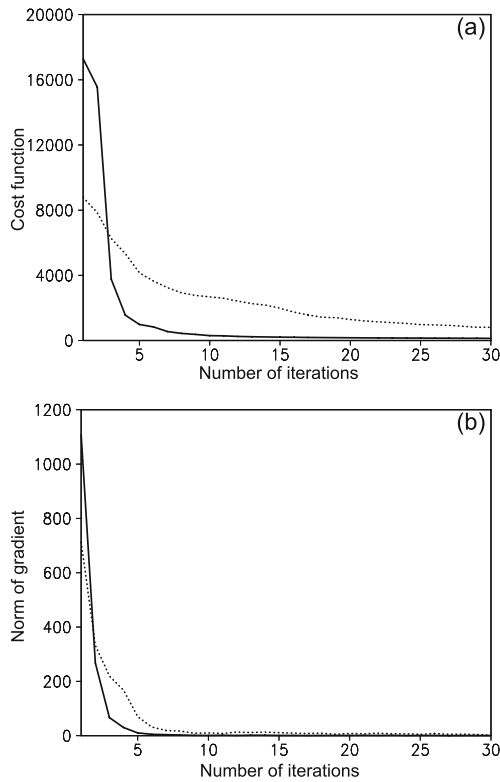
Fig. 5. (a) Cost function J and (b) norm of gradient G with respect to the number of iterations. The solid line is for PW3, and the dashed line is for Rain3.
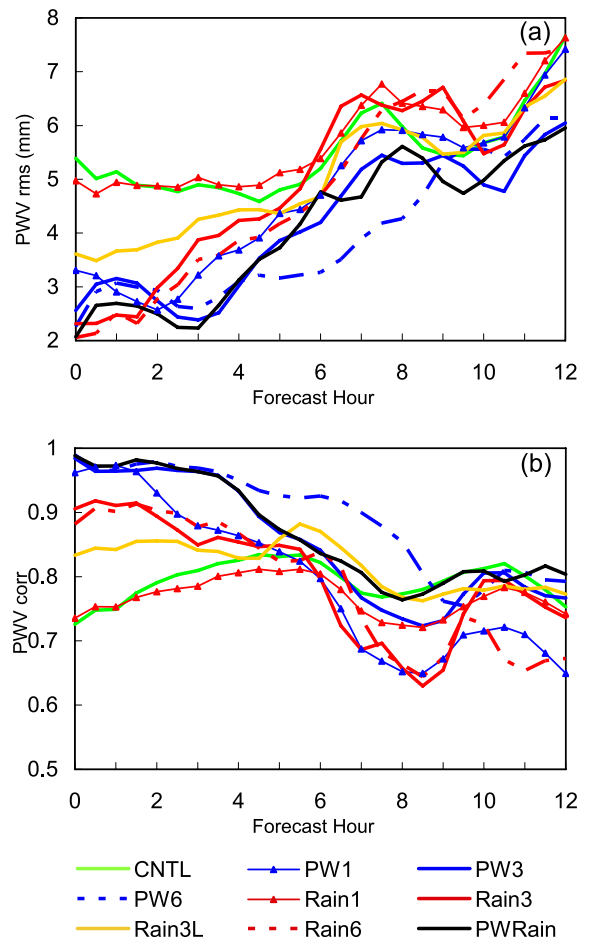

Fig. 6. Time series of (a) the average rms error and (b) the correlation coefficient of the model-derived PWV against 20 sites of observed GPS-PWV from 1200 UTC to 2400 UTC 20 June 2002.

indicating the improvements in the short-range moisture forecasts with the 4DVAR assimilations of either PWV or rainfall (Fig. 6a, b). The correlation in the GPS-PWV assimilation experiments are on average higher than that observed in the rainfall assimilation experiments (Fig. 6b), most likely because PWV has a more direct and linear observation operator H to the moisture field (Kuo et al., 1996), while the rainfall operator involves more complex model physics including the cumulus scheme (Zou and Kuo, 1996).

The effect of 4DVAR data assimilation, in terms of PWV error reduction, gradually reduced beyond the assimilation windows for most experiments. There are likely two main reasons for such reductions: firstly, the use of LBCs from a one-way nested coarse domain forecast while the fine domain was limited in size (e.g., Warner et al., 1997); secondly, errors in model physics that will become increasing more important in comparison with IC errors as the lead forecast times increase. Similarly, it is true for the CNTL, whose RMS error also increased slowly after 6 h (Fig. 6a).

Despite that additional (rainfall) observations were assimilated, the RMS errors and correlation coefficients in PWRain are very similar to those in PW3, because the J_{obs} term was weighted by the GPS-PWV

much higher than the hourly rainfall data in the current 4DVAR framework. Tuning the weightings of the observations based on different statistical assumptions could obtain various assimilation results, however, would not improve the forecast skills on the moisture field in the study. In practice, accurate estimates of error statistics depend upon observational errors, network density, range and other factors, which are not readily available.

4.3 MCS evolution

In this section, we select PW3 and Rain3 (which are among the best in Fig. 6) as examples to assess the impacts of 4DVAR assimilation on the predictions of the MCS evolution. The 1-h accumulated precipitation and the column maximum radar reflectivity valid at 1300, 1700, 2100, and 2400 UTC 20 June 2002 for CNTL, PW3 and Rain3 are illustrated in Figs. 7–9, respectively.
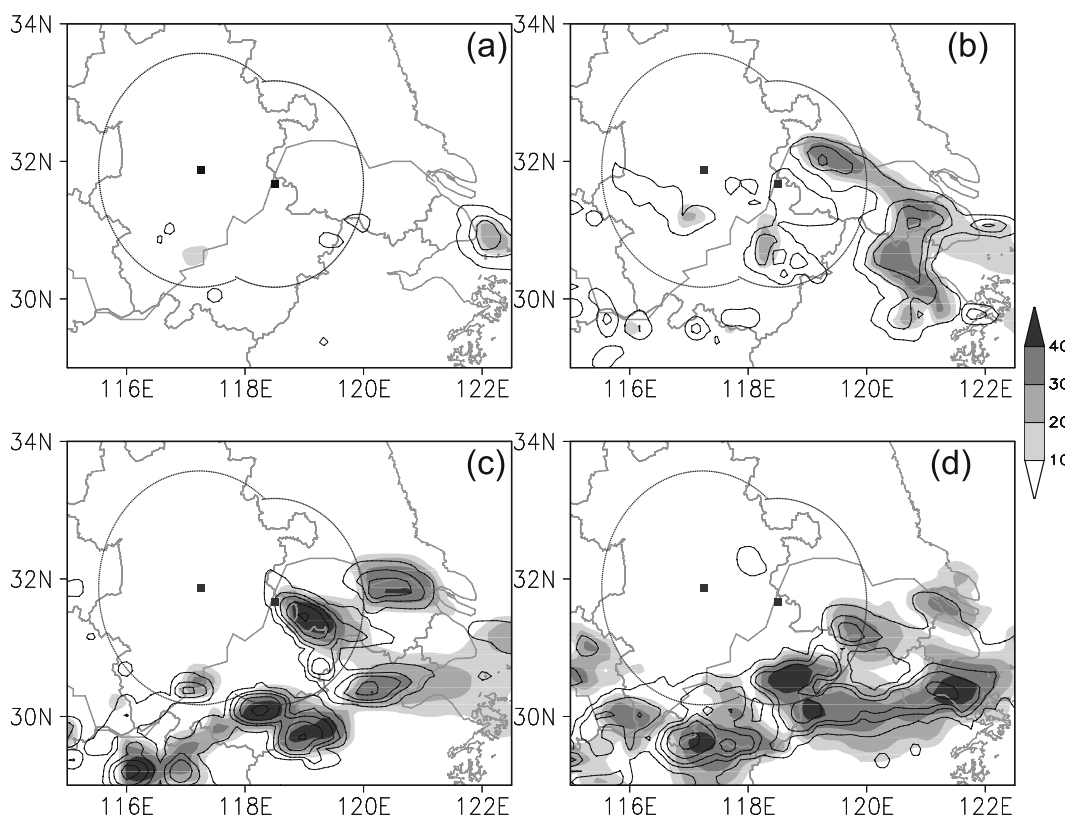
Fig. 7. Model output column maximum radar reflectivity images and 1-hour accumulated precipitation ending at (a) 1300 UTC, (b) 1700 UTC, (c) 2100 UTC, (d) 2400 UTC 20 June 2002, from the CNTL experiment. The contour intervals are the same as in Fig. 2.

CNTL without 4DVAR assimilation failed to predict either the generation at 1300 UTC (Fig. 7a) or subsequent intensification (Fig. 7b) of MCS A (refer to Figs. 2a–b) and produced some erroneous rainfall systems around Shanghai with the maximum precipitation over 20 mm (Figs. 7a-b). Although it did capture a general clustered pattern of the MCS rainfall at 2100 UTC (Fig. 7c), the evolution of MCSs B and C are far from accurate with big errors in both position and intensity. In the last hour of the simulation, the rainfall band deviated too far south from the observations (Fig. 7d) with heavy precipitation along the 30°N line.

With the 4DVAR assimilation of GPS-PWV, some dramatic improvements were found in the prediction of the MCS evolution in PW3 (Fig. 8). During the first 6 h, MCS A was successfully captured in terms of both its generation near the Dabie Mountains at 1300 UTC and its subsequent strengthening and eastward movement over the next 4 hours (Figs. 8a–b). At 1700 UTC, the forecasted MCS A was located at (31.2°N, 117°E) with over 20 mm precipitation, which agreed well with observations (Fig. 2b). The erroneous rainfall systems produced by CNTL (Figs. 7a,

b) were also eliminated. Also, MCSs B and C were initiated over the Huangshan Mountain region at this time (Fig. 8b) which quickly intensified over the next few hours. At 2100 UTC, the position, orientation and rainfall pattern of the MCS cluster (Fig. 8c) compared much more favorably with the observations than CNTL. Nevertheless, the PW3 forecast is not perfect at this time: MCS A was still too far westward and the simulated rainfall in all three MCSs was larger than the observations. At 2400 UTC (Fig. 8d), PW3 simulated the eastward propagation of these MCSs with much better rainfall forecast than the CNTL, but MCS B was slightly farther to the south and MCS C was too far to the east compared to the observations. In summary, with the 4DVAR assimilation of GPS-PWV, PW3 simulated the evolution of these MCSs over the lower reaches of Yangtze River much better than the CNTL, however, the rainfall amount was sometimes over predicted.

Similar to PW3, the Rain3 experiment assimilated hourly rainfall observations instead of GPS-PWV (Fig. 9). For the first 6 h, Rain3 performed similarly to PW3 in initiating MCS A and avoiding the erroneous rainfall systems found in the CNTL experiment that
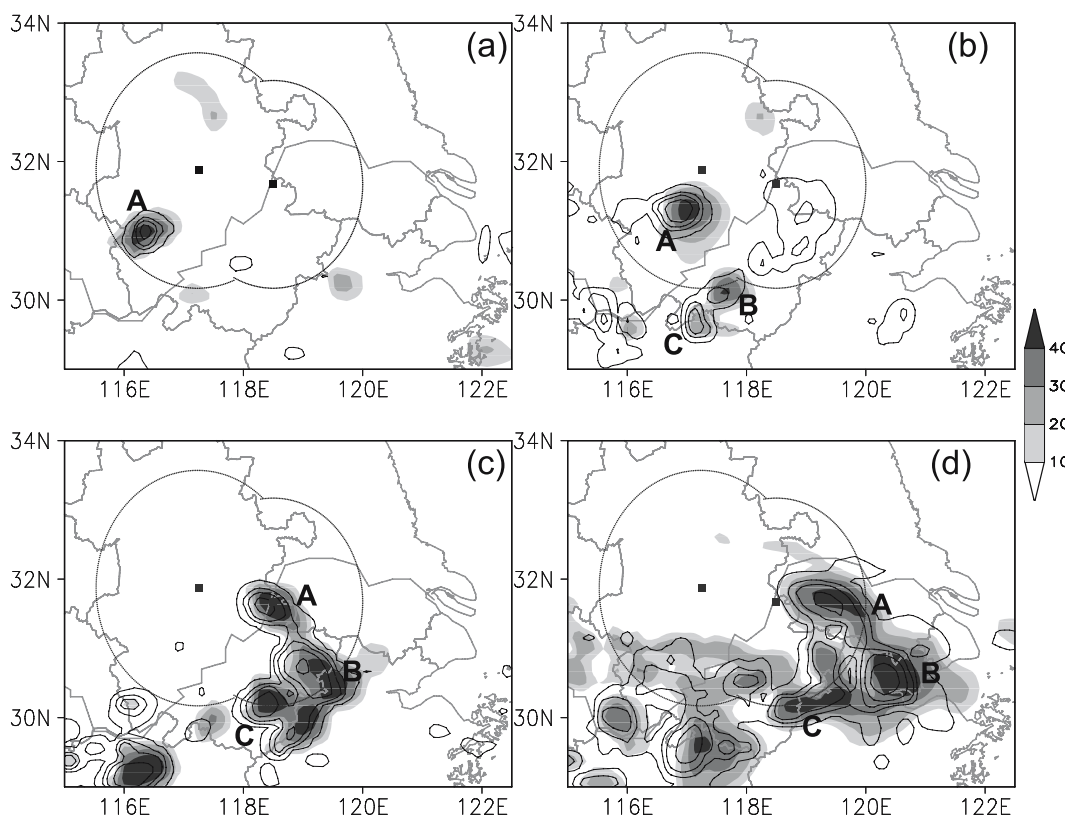
Fig. 8. As in Fig. 7 but for PW3 experiment.

occurred over the vicinity of Shanghai (Figs. 9a–b vs. Figs. 7a–b). Despite a better initial position in Rain3 than PW3 at 1300 UTC, MCS A in Rain3 moved too far to the north and weakened too quickly after 1700 UTC when compared to observations (Fig. 9c). The difference between Rain3 and CNTL, and thus the assimilation impacts on rainfall prediction, were rather insignificant in the last forecast hours, because both of them predicted MCSs B and C in the wrong places at 2400 UTC (Fig. 9d). Possible reasons for the rather small improvement with rainfall assimilation, especially in the later period of the simulation, are: (1) MCS A during the 3-h assimilation window developed so quickly and propagated so fast that the hourly accumulated rainfall observations might not contain sufficient information to adjust the ICs properly through the current assimilation scheme (Zou and Kuo, 1996; Zou, 1997) (detail in section 5.2); and (2) there were apparent spurious gravity waves in the 4DVAR-adjusted ICs of Rain3 (detail in section 5.3), which could potentially degrade its performance.

For other 4DVAR experiments (not shown), examinations of the evolution of the MCSs and associated rainfall centers showed that PW1, PW6 and PWRain performed similarly to PW3, Rain3L and Rain6 were similar to Rain3, while Rain1 was similar

to the CNTL, only with small variations in the MCS patterns, which are consistent to Fig. 6.

5. 4DVAR adjustments on initial conditions

In this section we examine what are the key changes in the ICs that led to the improved performance in the simulations with 4DVAR assimilation of PWV and/or rainfall observations. Instead of directly examining the IC differences of a few control variables (e.g., u, v, w, T, q) between simulations with and without 4DVAR at selected model layers, we attempt to diagnose the IC adjustments in terms of a few model-derived variables including the precipitable water vapor, moisture flux and equivalent potential temperature, which are more representative and integrated factors of the complicated MCS dynamics and physics. We will also attempt to reveal the limitations in the current 4DVAR algorithm, especially in its generation of spurious gravity waves. For brevity, only the changes in the ICs of PW3 and Rain3 are examined in detail.

5.1 *Moisture distribution and transport*

This study focuses on the initial moisture distribution and subsequent rainfall forecasts. Three compre-
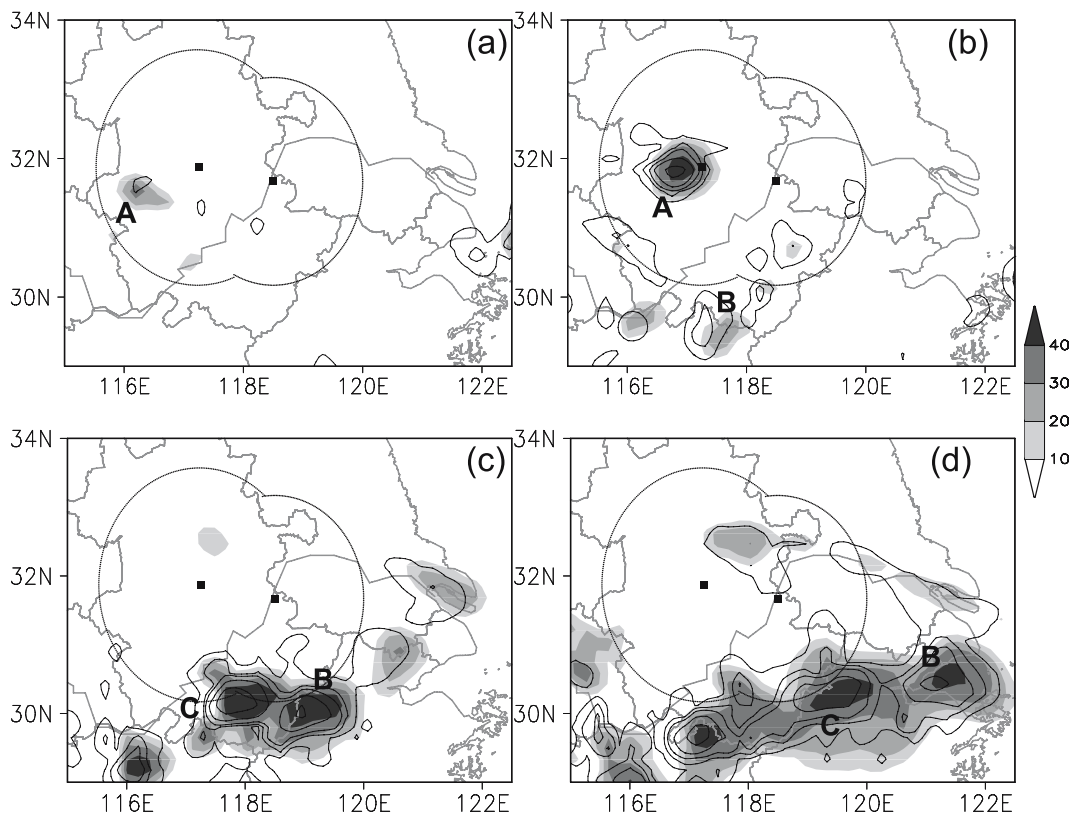
Fig. 9. As in Fig. 7 but for Rain3 experiment.

hensive variables were used, namely, PWV (Fig. 10, which represents the total amount of atmospheric water vapor), the moisture flux (Q) and the equivalent potential temperature at 850 hPa (θ_e, Fig. 11). In particular, we use the 350-K θ_e contour to represent the southern boundary of the meiyu front (Figs. 10, 11) because this front usually develops along a shear line with high θ_e gradients (Chen et al., 1998), which is along the 350-K θ_e contour at 850 hPa in this case.

The initial PWV distributions in PW3 and Rain3 ICs and their differences in comparison to CNTL are displayed in Figs. 10a, b. Both experiments compared well with observations as indicated by the low RMS errors and high correlations (2.6 mm, 0.98 for PW3 and 2.3 mm, 0.91 for Rain3), which are much better than those (5.4 mm, 0.72) found in CNTL (Fig. 6). They are also consistent with each other in the patterns and the PWV centers, which were both near (31.5°N, 117°), though differed in their maximum values. The major IC changes occurred along the 31°N line compared to CNTL, which may erroneously have too much PWV in the area (refer to large negative values in Figs. 10a, b) and then result in the erroneous rainfall systems observed in the CNTL experiment (Figs. 7a, b). Both PW3 and Rain3 also had higher PWV than CNTL (positive differences in Figs.

10a, b) near the Dabie Mountains region, which corresponds well with the better positions of MCS A generation (Figs. 8a, 9a). There is also a larger positive region of PWV difference in PW3 on the northern side of the mei-yu front around the 33°N line that is due to the increased background moisture in this area after the PWV assimilation and does not seem to have any direct effects on the MCS rainfall events. However, since the MCS does not usually initiate over the high PWV center, the improvements of the 4DVAR assimilation come from the overall PWV distribution, rather than localized maxima. On the other hand, there is a common belief that the PWV time series could be used to predict the trend of the precipitation, since PWV increasing usually precedes the rainfalls. But this is not true for the current heavy rainfall event, because the background PWV values persisted on a high level (over 60 mm) in the lower reaches of the Yangtze River throughout the 2002 mei-yu season and the correlation between PWV trend and precipitation was weak (not shown).

There are three crucial elements for heavy rainfalls along the mei-yu front, namely, moisture advection, vertical motion and instability (Ding, 1992; Chen et al., 1998). Differences in and θ_e primarily reflect the changes of moisture and heat transportation. In the
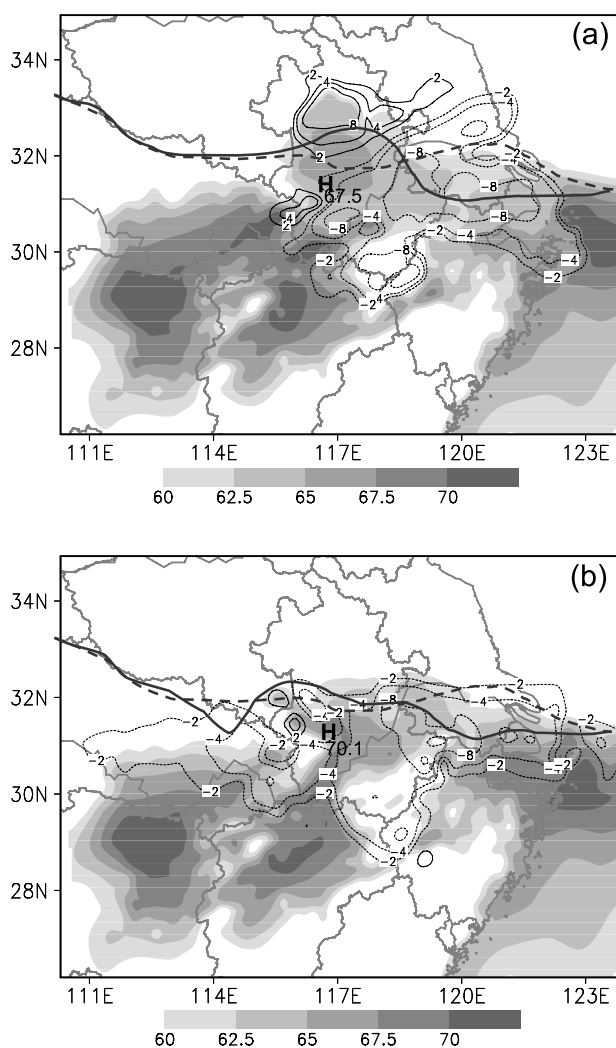
Fig. 10. The difference field of model output PWV at 1200 UTC 20 June 2002 (solid for positive areas, dashed for negative areas), (a) between PW3 and CNTL, (b) between Rain3 and CNTL. The intervals are ± 2, ± 4, ± 8 mm. The shaded areas respectively indicate the model-derived PWV fields of PW3 IC and Rain3 IC (mm). The highlighted 350-K θ_e line is dashed for CNTL, and solid for assimilation experiments.

initial stages of an MCS, a southwesterly mesoscale Low-Level Jet (mLLJ) usually forms at its southern side, which brings warm moist air to support its development (Chen et al., 1998). The intensifying (weakening) mLLJ usually enhances (discourages) the MCS initiation. IC changes in moisture and wind fields after 4DVAR assimilation of the GPS-PWV in PWV3, led to better positioning and shaping of the mei-yu front within the observational network (Fig. 11a). We noticed that: the two positive areas of θ_e and increments (over 4 K and 0.02×10^{-7} s^{-1}), which represent the increased background moisture and a strengthen-

ing mLLJ, contribute to the northward correction of the mei-yu front; the negative areas (over -4 K and -0.03×10^{-7} s^{-1}) that lie on the southward receding regions of the front, indicate the background moisture reduction and a weakening mLLJ. For instance, the intensified mLLJ over the Dabie Mountains signified the moisture and latent heat transports in this region, which led to the MCS A genesis (Fig. 8a). On the contrary, based on the trajectory analysis of the erroneous rainfall systems in CNTL, we find that the large areas of the reduced θ_e and weakened mLLJ acted to reduce the moisture transport and therefore prevented the generation of the erroneous systems in PW3 that were observed in the CNTL experiment (Figs. 7a, b).

In Rain3 (Fig. 11b), the rainfall assimilation also made some similar IC modifications, but with a larger magnitude. The absolute values of θ_e, changes were more than 8 K and 0.06×10^{-7} s^{-1} (both compared to CNTL). However, the area of the northward extension was smaller than it was in PW3, which is likely due to the inconsistency between the assimilated GPS-PWV and the hourly rainfall observations (also refer to Fig. 10). Similar to PW3, Rain3 also captured the initial perturbations of MCS A and eliminated the erroneous rainfall systems (Figs. 9a, b), but the modified fields of θ_e and after rainfall assimilation disagreed with each other over the positive regions where the MCS A was generated. The increased latent heat (θ_e) enhanced the convective instability for the MCS genesis, but the moisture flux increments did not indicate a strengthening mLLJ, in fact, it had a rather noisy divergent trend that should degrade the MCS development. The noisy divergent moisture flux revision may come from the spurious gravity waves, as a result of the imbalance between the wind and mass fields, which were not well constrained by the model dynamical laws in the 4DVAR assimilation of rainfall data.

5.2 *Vertical motion and instability*

To further understand the IC modifications with the 4DVAR assimilation that led to the improved forecasts, we examined the vertical motion and static instability along the cross section (located along the 116.3°E line) through MCS A in different experiments (Figs. 12–13). The CNTL (Fig. 12a), which was directly interpolated from the NCEP-FNL data without 4DVAR, did not display a high-θ_e plume, which would represent the strong convective instability and usually coincides with strong upward motions of the MCSs, instead only a weak synoptic-scale updraft above the mei-yu front at about 33°N was observed. It indicates that the ICs of CNLT lacked the right mesoscale perturbations to initiate the MCSs (Fig. 7a).

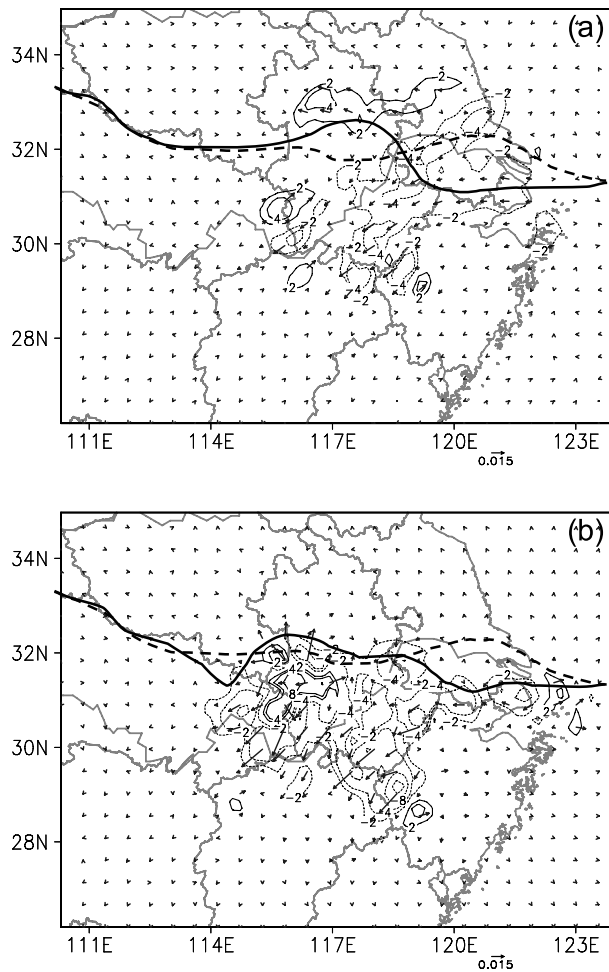With 4DVAR assimilation of the GPS-PWV, the

Fig. 11. The difference field of the moisture flux (isotach is 0.015×10^{-7} s^{-1}) and equivalent potential temperature (contour intervals are ± 2, ± 4, ± 8 ± 12 K) at 850 hPa between Optimal IC and CNTL IC on 1200 UTC 20 June 2002, (a) for PW3 and (b) for Rain3. The highlighted line is the same as in Fig. 10.

ICs of PWV3 captured the high-θ_e plume at the correct location of MCS A initiation (Fig. 12b), which provided a favorable, unstable condition for the MCS development with most of the changes found in the thermodynamic fields rather than the wind fields. For example, the value of convective available potential energy (CAPE) at (31°N, 116.3°E) in PW3 is 560 J higher than it in CNTL, despite there being only very small differences in u, v, and w. The mesoscale moisture perturbations with unstable stratification quickly triggered MCS A with strong updrafts during the beginning hours of the forecasts. At 1300 UTC (Fig. 13a), the maximum differences in the horizontal and vertical winds were more than 4 m s^{-1} and 1.2 m s^{-1} with pronounced mesoscale convection at 31°N, respectively. In the meantime, the updraft further en-

hanced the high-θ_e plume, with a much greater difference (i.e., 1240 J) in CAPE between PW3 and CNTL.

The high-θ_e plume of MCS A was also produced by rainfall assimilation in Rain3 IC (Fig. 12c), but with some noted differences: (1) the center of MCS A was located at about 31.6°N in Rain3, slightly further north of that was found in PW3; (2) the modifications in moisture and temperature (and thus instability) concentrated mostly at the lower levels with much greater changes in magnitude than those observed in PW3 [e.g., maximum CAPE difference is 1860 J at (31.6°N, 116.3°E)]; and (3) the maximum changes in the horizontal winds were 4 m s^{-1} while the vertical motion changes remained very small. The IC changes led to rapid development of MCS A after 1-h forecasts with an apparent downdraft and accompanying cold pool, but the maximum CAPE difference of MCS A quickly reduced to 1410 J at 1300 UTC (Fig. 13b). This suggests that the current 4DVAR assimilation of rainfall in Rain3 forced the MCS to develop much too quickly, which is not favorable for its further development and sustainability.

For better reduction in the cost function (section 3.3), Rain3 uses the Anthes-Kuo scheme for rainfall assimilations, in which the moistening and heating effects of the convections are determined through the help of the empirically normalized, vertical profiles (Zou and Kuo, 1996; Zou, 1997). This implies that the IC modifications are designed to satisfy the parameterization convection rather than the true atmospheric state. The representativeness and effectiveness of the assumed empirical profiles depends strongly upon the model resolutions and the weather events. The apparent over-correction of the initial low-level high-θ_e plume in Rain3 was likely a reason of forcing the model variables to produce more localized precipitation under the cumulus scheme rather than the true atmosphere. This problem persists for all 4DVAR experiments with rainfall assimilation in the current study and remains one of main obstacles in assimilating rainfall observations.

5.3 *Spurious gravity waves*

As mentioned in section 5.1, there may be a dynamical imbalance in the modified ICs with rainfall assimilation, which could lead to unphysical or spurious gravity waves in the ICs and also the early forecast hours. However, they are most likely unphysical in nature, high in frequency, hard to predict and often nonlinearly interact with the true physical features, all of which would degrade the effectiveness and efficiency of the data assimilations (page 186, Kalnay, 2003). The IC imbalance can be evaluated through diagnosis of the horizontal divergence and the residual of the non-
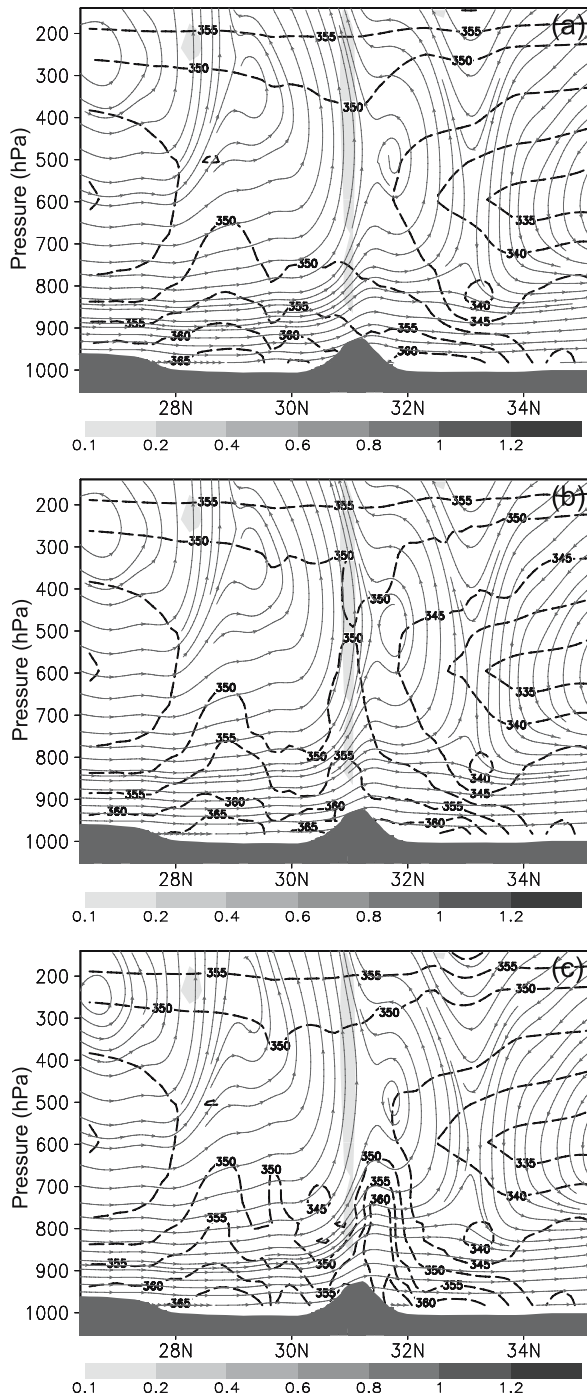
Fig. 12. The meridional-vertical cross-section of the equivalent potential temperature θ_e (long dashed line) and streamline (solid line with arrow) perpendicular to MCS A at 1200 UTC 20 June 2002 for (a) CNTL, (b) PW3 and (c) Rain3. The contour interval is 5 K for θ_e. The vertical velocity (shaded) in m s^{-1} is also displayed.

where J is the Jacobian term, $\beta = \partial f/\partial y$, Φ is the geopotential height and ζ is the relative vorticity, respectively (Zhang et al., 2001).

There is clear evidence of the imbalance and strong, northward propagating, spurious gravity waves in the ICs of Rain3 (Fig. 14b) and Rain3L (at a reduced amplitude due to a smaller observation weighting; Fig. 14c), but the imbalance and spurious waves are not evident in the ICs of PW3 and PW6 (Figs. 14a, d). However, after the 1-h forecasts, only PW3 developed the MCS normally (Fig. 14e), while the other experiments were all affected by the spurious gravity waves to some extent. Even though the IC noises of Rain3 and Rain3L are quite different, the spurious gravity waves in the 1-h forecast fields are nearly identical in terms of propagation and intensity (Figs. 14f, g), suggesting the dynamical imbalance features in their ICs have similar influences on the predictions. The spurious waves also quickly developed in the forecasts of PW6, propagated easterly from Dabie Mountains with
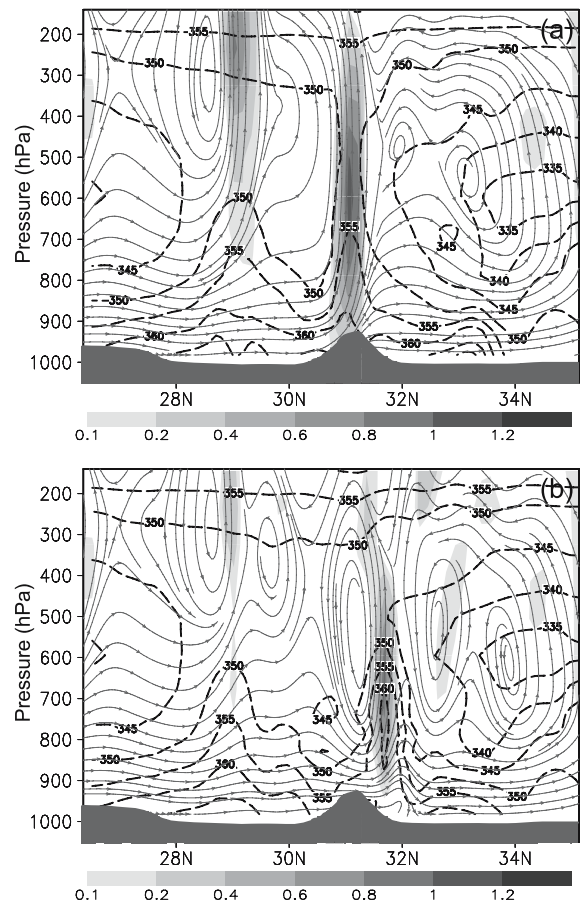

Fig. 13. The meridional-vertical cross-section perpendicular to MCS A at 1300 UTC 20 June 2002, (a) for PW3 and (b) for Rain3. The legend is the same as Fig. 12.
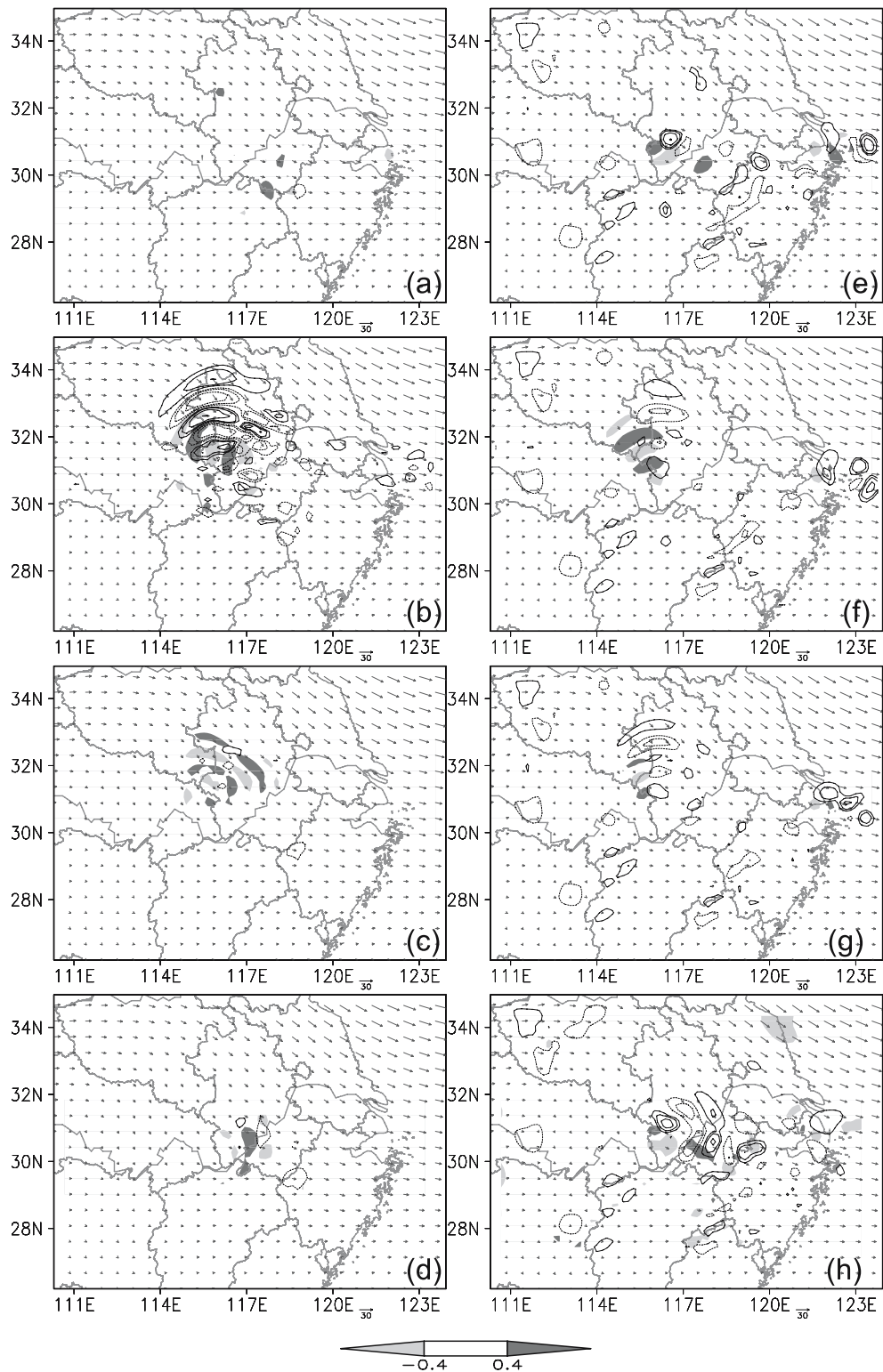
linear balance equation (ΔNBE) (Fig. 14):

$$\Delta\text{NBE} = 2J(u,v) + f\zeta - \nabla^2\Phi - \beta u \,, \qquad (3)$$

Fig. 14. The horizontal wind (isotach is 30 m s^{-1}) and divergence [intervals are (± 5, ± 10, ± 20, ± 40) $\times 10^{-5}$ s^{-1}] fields at 250 hPa. The shaded areas are the residual of the nonlinear balance equation in assimilation experiments against CNTL (unit: 10^{-8} s^{-2}; dark grey: positive; light grey: negative). (a), (b), (c), (d) are for PW3, Rain3, Rain3L and PW6, respectively, at 1200 UTC 20 June 2002 and (e), (f), (g), (h) are for PW3, Rain3, Rain3L and PW6 at 1300 UTC, respectively.

large amplitude (Fig. 14h). In fact, the spurious gravity waves also correlate with the unusual MCS dissipation in Rain3, Rain3L and PW6, suggesting the adverse impacts of these waves on subsequent forecasts.

The existence of spurious gravity waves may be related to several possible factors in the 4DVAR system. For rainfall assimilation, the cumulus parameterization scheme plays an essential role in the minimization procedure, which typically consists of "on-off" switches that represent strong nonlinearity and discontinuity in the observation operators (Zupanski and Mesinger, 1995; Xu, 1996a,b; Zou, 1997). The current linearization algorithm might be a significant source of assimilation errors in the 4DVAR system due to unavoidable violations of physics represented by those switches. The gradient of the CF, which is provided by the associated ADM, sometimes is not consistent with the original nonlinear forecast solution. Such inaccurate CF gradient computations would introduce imbalances in the ICs by producing small-scale noises (i.e., spurious gravity waves) in the current parameterization schemes (Vukićević and Bao, 1998). The amplitude of these noises is closely related to the observation weightings. With this limitation, the positive impacts of the rainfall assimilation on the prediction of MCS evolutions may be degraded sometimes due to these spurious gravity wave noises.

A longer assimilation window is also likely to make erroneous IC corrections, owing to both the "perfect model" assumption of 4DVAR system and the observational errors. For example, by assimilating PWV over a 6-h period (doubled that of PW3), PW6 was also affected by the spurious gravity waves. For the first aspect, the premise of the current 4DVAR algorithm presented in formula (1) is that the forecast model is perfect, which means to give the same credence to all of the observational increments during the assimilation window (Menard and Daley, 1996). In fact, the forecast uncertainties from the model errors should also be included in J_{obs} through combining the model error covariance matrix with O^{-1} or adding an independent mode error term to constrain the CF (Zupanski, 1997). Moreover, observational errors induced by the instrument accuracy and representativeness (incomplete observations for the MCS) might also contaminate the assimilation results with unrealistic perturbations. The longer window the larger amount of errors would be accumulated during the minimization. In practice, there is a lack of accurate estimations for the observation and background error weightings without sufficient statistical information. Both model errors and uncertainties in observation weightings may exist in the current 4DVAR framework, which could lead to inaccurate representation of CF and the subsequent spurious gravity waves, especially for the rainfall assimilation.

There have been several attempts to eliminate these imbalanced noises: Lynch and Huang (1992, 1997) proposed the Digital Filter Initialization method to filter out the fast oscillations, which is easy to implement for limited-area models, while some other researchers (Polavarapu et al., 2000; Gauthier and Thépaut, 2001; Wee and Kuo, 2004) used a digital filter to force the 4DVAR system to only use the low-frequency meteorological waves to fit the observations, instead of the high-frequency gravity waves that would rapidly disperse, where a penalty term was introduced in CF to prevent those spurious gravity waves. It may also be beneficial to add wind observations while assimilating PWV and rainfall to constrain the wind fields, which are usually connected with the imbalance features (Guo et al., 2000; De Pondeca et al., 2001).

6. Sensitivity experiments

Verifications of the moisture fields for all experiments shown in Fig. 6 demonstrated the success of the 4DVAR assimilation is very sensitive to the observations assimilated, assimilation windows and observation weightings. More specifically, PW1 and PW3 (assimilating PWV) with a relatively short assimilation window performed similarly (well) in terms of RMS error and correlation coefficient, both are better than CNTL without 4DVAR for the first few hours of the forecast, but the advantages over CNTL began to diminish after 6 h. With a longer assimilation window, the impacts of 4DVAR assimilation of more GPS-PWV in PW6 persisted for almost 9 h, which is especially noteworthy after 4-h forecasts. It indicates that the impacts of the GPS-PWV assimilation on moisture prediction are highly correlated with the assimilation windows: a short window could rapidly and faithfully reduce the prediction errors in the first 6 h but an extended window would further extend the improved prediction on the moisture field.

This is not true for rainfall assimilation: the forecast skills of Rain3 and Rain6 are almost the same within the 12-h period. On the other hand, no obvious forecast improvements in Rain1 were observed since the ICs change was small due to very little precipitation being observed and assimilated during the 1-h assimilation window (refer to Figs. 2a and 7a; also in Zou and Kuo, 1996).

Tuning the observation weightings can also lead to significant differences in the 4DVAR performance. For example, Rain3L with the reduced observation weighting resulted in higher RMS errors and lower correlation in the first 6 h. Indeed, the observation weighting

of rainfall data, which depends on the variety of measurements and weather conditions, is a tunable parameter in the 4DVAR algorithm. Improved forecasts with rainfall assimilation are reported in literature (e.g., Zupanski and Mesinger, 1995; Zou and Kuo, 1996; Guo et al., 2000), but with much different observation weightings. The weighting in Rain3 performed the best for this study.

7.   Summary and Conclusions

This study examined the impacts and sensitivity of GPS-PWV and hourly rainfall assimilation with the MM5 4DVAR system on the prediction of MCS evolution for a heavy rainfall case during the 2002 mei-yu season. With the successful assimilation of the GPS-PWV data (e.g., PW3), significant forecast improvements (over the experiment without 4DVAR) were obtained throughout the entire 12-h simulation, which not only reproduced the initiation and evolution of the MCS clusters, but also eliminated the erroneous rainfall systems that were observed in the CNLT experiment. Experiments with rainfall assimilation also obtained some improved MCS forecasts, but the simulated precipitation was too localized and dissipated too quickly when compared to the observations. This might be due to the limitations of the cumulus parameterization that was used in 4DVAR procedures and/or the introduction of spurious gravity waves. The three-dimensional moisture structure and the mei-yu front within observational network were much better represented in the ICs with the 4DVAR assimilation. Diagnosis of the IC differences in moisture flux (Q) and equivalent potential temperature (θ_e) showed that experiments with 4DVAR assimilation obtained improved low-level moisture perturbation and an intensified mLLJ, which could support the MCS development. The GPS-PWV assimilation was extremely beneficial to improve the initial moisture analysis.

The efficiency of GPS-PWV and rainfall assimilations may be degraded by the introduction of spurious gravity waves in different extents. Longer assimilation windows and bigger weighting would aggravate the amplitude of these noises. Even though the model dynamics and physics are used as strong constraints, there are still many assumptions and approximations in the current 4DVAR framework, especially those of the "perfect-model" assumption and "on-off" switches. The observational errors could also introduce some undesirable IC adjustments when such error statistics can not be sufficiently obtained.

The improved forecasts of the moisture field were sensitive to assimilation windows in the GPS-PWV assimilation: even a 1-h assimilation window can lead to an improved prediction, but an extended window is needed to enhance the benefits. The efficiency of the rainfall assimilation does not strongly depend on the assimilation window, but is very sensitive to observation weightings, which are tunable for different measurements and weather events.

Our studies on GPS-PWV and rainfall assimilations were generally successful, but there are several unresolved issues: (1) even though the rainfall pattern and evolution of the MCS were predicted well following the GPS-PWV/rainfall assimilations, the precipitation was usually over-predicted; (2) we do not have sufficient error statistics of the background and the observations to define the optimal covariance matrices, which is an essential part of the 4DVAR system and often needs flow-dependent information; (3) the lateral boundary conditions (LBC) might also have strong impacts on the limited-area model forecasts, which could have been incorporated into the minimization process of CF (Zou and Kuo, 1996); (4) effective control of spurious gravity waves are needed for the current 4DVAR algorithm; (5) GPS-PWV and rainfall assimilations actually have similar contributions to the moisture field, but lack effective modifications on the three-dimensional wind. The wind observations, such as those from the profiler and radar radial velocity observations, may be assimilated synchronously to improve the accuracy of the 4DVAR adjustments. All of these problems will be investigated in our future works.

REFERENCES

Bevis, M. S., S. Businger, T. A. Herring, C. Rocken, R. A. Anthes, and R. H. Ware, 1992: GPS meteorology: Remote sensing of atmospheric water vapor using the global positioning system. *J. Geophys. Res.*, **97**, 15787–15801.

Blackadar, A. K., 1979: High resolution models of the planetary boundary layer. *Advances in Environmental Science and Engineering*, Vol. 1, J. R. Pfafflin and E. N. Ziegler, Eds., Gordon and Breach, 50–85.

Braun, J., C. Rocken, and R. Ware, 2001: Validation of line-of-sight water vapor measurements with GPS. *Radio Sci.*, **36**, 459–472.

Chen S., Y. H. Kuo, W. Wang, Z. Tao, and B. Cui, 1998: A modeling case study of heavy rainstorms along the mei-yu front. *Mon. Wea. Rev.*, **126**, 2330–2351.

Courtier, P., and O. Talagrand, 1987: Variational assimilation of meteorological observations with the adjoint vorticity equation. Part II. Numerical results. *Quart. J. Roy. Meteor. Soc.*, **113**, 1329–1368.

Davison, N. E., K. Kurihara, T. Kato, G. Mills, and K. Puri, 1998: Dynamics and prediction of a mesoscale extreme rain event in the baiu front over Kyushu, Japan. *Mon. Wea. Rev.*, **126**, 1608–1629.

De Pondeca, S. F. V. Manuel, and X. Zou, 2001: A case study of the variational assimilation of GPS zenith delay observations into a mesoscale model. *J. Appl. Meteor.*, **40**, 1559–1576.

Ding, Y., 1992: Summer monsoon rainfalls in China. *J. Meteor. Soc. Japan*, **70**, 337–396.

Duan, J. P., and Coauthors, 1996: GPS meteorology: Direct estimation of the absolute value of precipitable water. *J. Appl. Meteor.*, **35**, 830–838.

Dudhia, J., 1989: Numerical study of convection observed during the Winter Monsoon Experiment using a mesoscale two-dimensional model. *J. Atmos. Sci.*, **46**, 3077–3107.

Gauthier, P., and J.-N. Thépaut, 2001: Impact of the digital filter as a weak constraint in the preoperational 4DVAR assimilation system of Météo-France. *Mon. Wea. Rev.*, **129**, 2089–2102.

Grell, G. A., 1993: Prognostic evaluation of assumptions used by cumulus parameterizations. *Mon. Wea. Rev.*, **121**, 5–31.

Grell, G. A., J. Dudhia, and D. R. Stauffer, 1994: A description of the fifth-generation Penn State/NCAR Mesoscale Model (MM5). Tech. Note TN-3981IA, National Center for Atmospheric Research, Boulder, CO, 125pp.

Guo, Y.-R., Y.-H. Kuo, J. Dudhia, D. Parsons, and C. Rocken, 2000: Four-dimensional variational data assimilation of heterogeneous mesoscale observations for a strong convective case. *Mon. Wea. Rev.*, **128**, 619–643.

Ha, S-Y, Y-H. Kuo, Y-R. Guo, and G-H. Lim, 2003: Variational assimilation of slant-path wet delay measurements from a hypothetical ground-based GPS network. Part I: Comparison with precipitable water assimilation. *Mon. Wea. Rev.*, **131**, 2635–2655.

Kalnay, E., 2003: *Atmospheric Modeling, Data Assimilation and Predictability.* Cambridge University Press, 341pp.

Kuo, H. L., 1974: Further studies of the parameterization of the effect of cumulus convection on large scale flow. *J. Atmos. Sci.*, **31**, 1232–1240.

Kuo, Y.-H., Y.-R. Guo, and E. R. Westwater, 1993: Assimilation of precipitable water measurements into a mesoscale model. *Mon. Wea. Rev.*, **121**, 1215–1238.

Kuo, Y.-H., X. Zou, and Y.-R. Guo, 1996: Variational assimilation of precipitable water using a nonhydrostatic mesoscale adjoint model. Part I: Moisture retrieval and sensitivity experiments. *Mon. Wea., Rev.,* **124**, 122–147.

Le Dimet, F.-X., and O. Talagrand, 1986: Variational algorithms for analysis and assimilation of meteorological observations: Theoretical aspects. *Tellus*, **38A**, 97–10.

Liu, D. C., and J. Nocedal, 1989: On the limited memory BFGS method for large scale optimization. *Math. Program.*, **45**, 503–528.

Lynch, P., and X.-Y. Huang, 1992: Initialization of the HIRLAM model using a digital filter. *Mon. Wea. Rev.*, **120**, 1019–1034.

Lynch, P., and X.-Y. Huang, 1997: The Dolph–Chebyshev window: A simple optimal filter. *Mon. Wea. Rev.*, **125**, 655–660.

Menard, R., and R. Daley, 1996: The application of Kalman smoother theory to the estimation of 4DVAR error statistics. *Tellus*, **48A**, 221–237.

Moteki, Q., H. Uyeda, T. Maesaka, T. Shinoda, M. Yoshizaki, and T. Kato, 2004: Structure and development of two merged rainbands observed over the East China Sea during X–BAIU–99. Part I: Meso-β-scale structure and development processes. *J. Meteor. Soc. Japan*, **82**, 19–44.

Navon, I. M., X. Zou, J. Derber, and J. Sela, 1992: Variational data assimilation with an adiabatic version of the NMC spectral model. *Mon. Wea. Rev.*, **120**, 1433–1446.

Parrish, D. F., and J. C. Derber, 1992: The National Meteorological Center's spectral statistical-interpolation analysis system. *Mon. Wea. Rev.*, **120**, 1747–1763.

Polavarapu, S., M. Tanguay, and L. Fillion, 2000: Four-dimensional variational data assimilation with digital filter initialization. *Mon. Wea. Rev.*, **128**, 2491–2510.

Reisner, J., R. J. Rasmussen, and R. T. Bruintjes, 1998: Explicit forecasting of supercooled liquid water in winter stoRMS using the MM5 Mesoscale Model. *Quart. J. Roy. Meteor. Soc.*, **124B**, 1071–1107.

Sun Jianhua, Zhang Xiaoling, Qi Linlin, and Zhao Sixiong, 2005: An Analysis of a meso-β System in a mei-yu Front Using the Intensive Observation Data During CHeRES 2002. *Adv. Atmos. Sci.*, **22**, 278–289

Thepaut, J.-N., D. Vasiljevic, P. Courtier, and J. Pailleux, 1993: Variational assimilation of conventional meteorological observations with a multilevel primitive equation model. *Quart. J. Roy. Meteor. Soc.*, **119**, 153–186.

Vukićević, T., and J.-W. Bao, 1998: The effect of linearization errors on 4DVAR data assimilation. *Mon. Wea. Rev.*, **126**, 1695–1706.

Warner, T. T., R. A. Petersen, and R. E. Treadon, 1997: A tutorial on lateral boundary conditions as a basic and potentially serious limitation to regional numerical weather prediction. *Bull. Amer. Meteor. Soc.*, **78**, 2599–2617.

Wee, T.-K., and Y.-H Kuo, 2004: Impact of a Digital Filter as a Weak Constraint in MM5 4DVAR: An Observing System Simulation Experiment. *Mon. Wea. Rev.*, **132**, 543–559

Xu, Q., 1996a: Generalized adjoint for physical processes with parameterized discontinuities. Part I: Basic issues and heuristic examples. *J. Atmos. Sci.*, **53**, 1123–1142.

Xu, Q., 1996b: Generalized adjoint for physical processes with parameterized discontinuities. Part II: Vector formulation and matching conditions. *J. Atmos. Sci.*, **53**, 1143–1155.

Zhang, D-L., and R. A. Anthes, 1982: A high-resolution model of the planetary boundary layer sensitivity tests and comparisons with SESAME-79 data. *J. Appl. Meteor.*, **21**, 1594–1609

Zhang, F., S. E. Koch, C. A. Davis, and M. L. Kaplan, 2001: Wavelet analysis and the governing dynamics of a large amplitude mesoscale gravity wave event along the East Coast of the United States. *Quart. J. Roy. Meteor. Soc.*, **127**, 2209–2245.

Zhang Lin, and Ni Yunqi, 2005: Four-Dimensional Variational Data Assimilation Experiments for a Heavy Rain Case During the 2002 IOP in China. *Adv. Atmos. Sci.*, **22**, 300–312.

Zhang Qinghong, K.-H. Lau, Y.-H. Kuo, and Chen Shoujun, 2003: A numerical study of a mesoscale convective system over the Taiwan Strait. *Mon. Wea. Rev.*, **131**, 1150–1170.

Zou, X., and Y.-H. Kuo, 1996: Rainfall assimilation through an optimal control of initial and boundary conditions in a limited-area mesoscale model. *Mon. Wea. Rev.*, **124**, 2859–2882.

Zou, X., I. M. Navon, and J. Sela, 1993: Control of gravitational oscillations in variational data assimilation. *Mon. Wea. Rev.*, **121**, 272–289.

Zou, X., Y.-H. Kuo, and Y.-R. Guo, 1995: Assimilation of atmospheric radio refractivity using a nonhydrostatic adjoint model. *Mon. Wea. Rev.*, **123**, 2229–2249.

Zou, X., 1997: Tangent linear and adjoint of "on/off" processes and their feasibility for use in 4-dimensional variational data assimilation. *Tellus*, **49A**, 3–31.

Zou, X., F. Vandenberghe, M. Pondeca, and Y.-H. Kuo, 1997: Introduction to adjoint techniques and the MM5 adjoint modeling system. NCAR Tech. Note TN-435-STR, 110 pp. [Available from National Center for Atmospheric Research, P. O. Box 3000, Boulder, CO 80307-3000.]

Zupanski, D., and F. Mesinger, 1995: Four-dimensional variational assimilation of precipitation data. *Mon. Wea. Rev.*, **123**, 1112–1127.

Zupanski, D., 1997: A general weak constraint applicable to operational 4DVAR data assimilation system. *Mon. Wea. Rev.*, **125**, 2274–2292.

Zupanski, M., 1993: A preconditioning algorithm for large-scale minimization problems. *Tellus*, **45A**, 478–492.